On observing acoustic backscattering from salinity turbulence

Louis Goodman[a)]
University of Massachusetts Dartmouth, School for Marine Science and Technology, 706 South Rodney French Boulevard, New Bedford, Massachusetts 02744-1221

Marcos M. Sastre-Córdova
Raytheon Company, Seapower Capability Center, 1847 West Main Road, Portsmouth, Rhode Island 02871

(Received 18 August 2010; revised 21 May 2011; accepted 7 June 2011)

It has been hypothesized that at sufficiently high levels of oceanic salinity turbulence it should be possible to observe acoustic backscattering. However, there have been limited *in situ* measurements to confirm this hypothesis. Using an autonomous underwater vehicle equipped with upward and downward looking 1.2 MHz acoustic Doppler current profilers and with turbulence and fine scale sensors, measurements were performed in a region of intense turbulence and a strong salinity gradient. The approach taken was to correlate variations in the backscattered acoustic intensity, I, with a theoretical acoustic backscattering cross section per volume for salinity turbulence, σ_s, to obtain an estimated scattering cross section per volume, σ_e. Results indicated that of order 50% of the observed region was characterized by salinity turbulence induced backscattering.
 [DOI: 10.1121/1.3605666]

PACS number(s): 43.30.Ft, 43.30.PC, 43.30.Re, 43.30.Zk [KGF] Pages: 707–715

I. INTRODUCTION

It has long been speculated (Goodman and Kemp, 1981; Seim *et al*., 1995; Lavery *et al*., 2003) that very high frequency acoustic backscattering techniques could be used to infer temperature and salinity turbulence. In the ocean, density and sound speed fluctuations, which arise from temperature and salinity fluctuations, induce acoustic impedance fluctuations which can result in the directional scattering of sound waves (Goodman, 1990). Laboratory experiments (Oeschger and Goodman, 2003) have confirmed acoustic scattering from temperature fluctuations. Recent theoretical and observational research (Seim *et al*., 1995; Lavery *et al*., 2003; Ross and Lueck, 2003; Ross *et al*., 2004, 2007) have suggested that there are oceanic regions where salinity fluctuations could be sufficiently large to be observable. Because the molecular salinity diffusivity is 100 times smaller than that of the molecular temperature diffusivity, the spatial scale of salinity induced turbulence is 10 times smaller than that of temperature (Tennekes and Lumley, 1972). This results in the typical frequency of maximum acoustic scattering in the ocean for salinity turbulence to be in the megahertz frequency range, as compared to the hundreds of kilohertz frequency range for temperature turbulence.

Previous work on acoustic scattering from turbulence has been mainly theoretical, with a limited amount of field observations, particularly for the case of salinity. The present work describes a correlation technique of utilizing a set of near coincident acoustic intensity and environmental measurements to extract the contribution of salinity turbulence from the received acoustic scattered signal.

The organization of this manuscript is as follows. In Sec. II, a brief summary of the theory of acoustic scattering from turbulence is presented. The platform used for observations, the T-REMUS autonomous underwater vehicle, is described in Sec. III. Observations from the Merrimack River Mixing and Divergence Experiment (MerMADE) are presented in Sec. IV. The statistical approach utilized to estimate the scattering cross section per volume for salinity turbulence is developed in Sec. V. Results are given in Sec. VI. Other potential sources of scattering are discussed in Sec. VII. Section VIII contains the summary and conclusions.

II. THEORETICAL BACKGROUND

Using the Born approximation for weak scattering, it can be shown that the scattering cross section per volume at acoustic wavenumber, κ, arising from temperature (T) and salinity (S) fluctuations can be written as (Lavery *et al*., 2003)

$$\sigma = \underset{I}{\sigma_T} + \underset{II}{\sigma_{TS}} + \underset{III}{\sigma_S} = 2\pi\kappa^4\left[A_T^2\Phi_T(K) + A_TA_S\Phi_{TS}(K) + A_S^2\Phi_S(K)\right], \quad (1)$$

with A_T and A_S containing terms representing the fractional changes in sound speed and density due to temperature and salinity changes, respectively; Φ_T, Φ_S are the three-dimensional wavenumber spectra of temperature and salinity turbulence; Φ_{TS} is the cross spectrum of temperature and salinity turbulence. For backscattering these spectra are evaluated at the Bragg wavenumber, $K = 2\kappa$. To obtain a specific form for the spectra the next step typically taken (Goodman and Kemp, 1981; Goodman, 1990) is to assume that the fluctuations are turbulent and use a classical turbulence model, which assumes local homogeneity and isotropy (Bathchelor, 1993; Tennekes and Lumley, 1972). Using the classical salinity turbulence model (Dillon and Caldwell, 1980) and the scattering equations from Lavery *et al*. (2003), it can be

a)Author to whom correspondence should be addressed. Electronic mail: lgoodman@umassd.edu

shown that the temperature and salinity turbulence induced scattering cross section terms I and III of Eq. (1) reduce to

$$\sigma_T = C_T \gamma_T, \tag{2a}$$

$$\sigma_S = C_S \gamma_S, \tag{2b}$$

where

$$C_{T,S} = (A_{T,S})^2 \frac{qk\sqrt{\nu}}{16}, \tag{3}$$

and

$$\gamma_{T,S} = \frac{\chi_{T,S}}{\sqrt{\varepsilon}} \exp[-4q(k/k_{T,S})^2], \tag{4}$$

with $\chi_{T,S}$ the rate of turbulent diffusion of the temperature, salinity fluctuations, respectively, and $k_{T,S}$, the temperature, salinity Batchelor wavenumber, defined as $k_{T,S} = (\varepsilon/\nu D_{T,S}^2)^{1/4}$; ε is the turbulent kinetic energy dissipation rate; $D_{T,S}$ is the molecular diffusivity of temperature and salt, respectively, in water; ν is the kinematic viscosity of water; and q, a dimensionless constant, estimated to be ~3.7 (Oakey,1982). Expressing the temperature and salinity induced scattering cross section per volume, $\sigma_{T,S}$, in the form of Eq. (2) isolates the role that the environment has on the scattering. The cross spectral term is more difficult to obtain in closed form but we can, following Lavery *et al*. (2003), estimate an upper bound for it, namely, $\sigma_{TS} < 2\sqrt{\sigma_T \sigma_S}$. Observations from the T-REMUS autonomous underwater vehicle during the Merrimack River Mixing and Divergence experiment will be used to estimate the terms in Eq. (1).

III. APPROACH: T-REMUS AUTONOMOUS UNDERWATER VEHICLE

The observational approach is to use the autonomous underwater vehicle (AUV), T-REMUS, shown in Fig. 1. T-REMUS is a custom designed REMUS 100 vehicle, manufactured by Hydroid Inc. of Pocasset, MA, containing the Rockland Microstructure Measurement System (RMMS), manufactured by RGL Consulting Ltd. of Victoria BC, Canada. It is mounted on the left side of the nose of the vehicle. On the right hand side of the nose is the FASTCAT Conductivity Temperature Depth (CTD) instrument, manufactured by Sea-Bird Electronics of Bellevue, WA. The vehicle has an upward and downward looking 1.2 MHz Acoustic Doppler Profiler (ADCP), manufactured by Teledyne RD Instruments of Poway CA, and a BB2F Combination Spectral Backscattering Fluorometer, manufactured by WET Labs of Philomath OR. In addition, the vehicle contains a variety of "hotel" sensors which measure pitch, roll, yaw, and other internal dynamical parameters.

This suite of sensors on T-REMUS allows quantification of the key dynamical and kinematical turbulent and fine scale physical processes. The turbulence measurements are made concomitantly with very high spatial resolution measurements of temperature, salinity, and depth. The BB2F sensor system measures chlorophyll-a fluorescence and optical backscattering at 470 and 700 nm wavelength. The turbulent and fine scale quantities which can be estimated from the data collected by the T-REMUS include: the turbulent dissipation rate, the temperature diffusion rate, fine scale velocity shear, and fine scale stratification and, hence, the gradient Richardson and buoyancy Reynolds numbers. In addition, the fine scale temperature/salinity relationship can be obtained. Below we provide more details on the T-REMUS measuring system suite.

FIG. 1. The T-REMUS autonomous underwater vehicle. T-REMUS is a custom designed REMUS 100 vehicle, manufactured by Hydroid Inc of Pocasset MA. The turbulence package, designed and manufactured by RGL Consulting Ltd. of Victoria BC, Canada, is mounted on the left side of the nose of the vehicle. On the right hand side of the nose is the FASTCAT Conductivity Temperature Depth (CTD) instrument, manufactured by Sea-Bird Electronics of Bellevue, WA. The vehicle has an upward and downward looking 1.2 MHz Acoustic Doppler Profiler (ADCP), manufactured by Teledyne RD Instruments of Poway, CA, and a BB2F Combination Spectral Backscattering Fluorometer, manufactured by WET Labs of Philomath, OR.

A. Rockland Microstructure Measurements System (RMMS)

The RMMS package, designed by RGL Consulting Ltd. of Victoria BC, Canada, is mounted on the left side of the nose of the vehicle, as shown in Fig. 1. It is housed in a pressure case of 6 cm diameter and is approximately 0.5 m long. It consists of two fast response thermistors to measure temperature and its derivative and two shear probes, mounted 26.94 mm apart from each other, on the front end of the

pressure case. The shear probes provide an output proportional to the cross stream velocity gradient, $\partial v/\partial x$, and vertical velocity gradient, $\partial w/\partial x$, where x is the along track distance. The electronics board of the RMMS supports a set of triaxial accelerometers oriented along the three principle axes of the pressure case, and a pressure transducer that provides both pressure and its derivative. The data are collected at a sampling rate of 500 Hz. Goodman *et al*. (2006) describe a technique of coherently subtracting all three components of accelerometer data from the shear data to obtain an optimal estimate of the turbulent dissipation rate, ε. Using this technique the underway effective noise floor for the dissipation rate, ε, is found to be less than 10^{-9} W/kg.

B. Conductivity, temperature, and depth (CTD)

The FASTCAT CTD manufactured by Sea-Bird Electronics, Inc. of Bellevue, WA, is mounted on the right front of T-REMUS. It is an integrated CTD sensor system specifically designed for usage by either a towed body or an AUV. The FASTCAT CTD has a pump-controlled, TC-ducted flow which minimizes salinity spiking. The 16 Hz sampling rate results in very high spatial resolution, typically of order centimeters. The *in situ* CTD collected temperature and depth data are used to calibrate temperature and depth data obtained from the RMMS probes.

C. Acoustic Doppler Current Profilers (ADCP)

The REMUS 100 AUV comes standard with two 1.2 MHz Workhorse Acoustic Doppler Current Profiler (ADCP) systems, one upward and one downward looking. These are manufactured by Teledyne RD Instruments of Poway, CA. Each ADCP contains four beams, oriented 20° to the vertical, with each 20° wide. In shallow water (<30 m) the system allows bottom tracking, which is used to estimate the vehicle speed and direction, and, thus, along with the water-borne returns, the water speed and direction. The 1.2 MHz ADCP sonar has a blanking distance of approximately 1.1 m. The ADCP also outputs uncalibrated acoustic intensity. In this work we use the averaged output intensity of the four beams. The ADCP pulse length is 0.5 m with a repetition rate (total over the consecutive upward and downward pulses) of 3.5 s. The uncalibrated noise level of the system is 24 dB. From the results of Sec. V it can be shown that this corresponds to a calibrated backscattering cross section per unit length floor value of −106 dB.

Only the first bin of the upward and downward sonar systems is used in our analyses. Employing this approach results in a consistent set of acoustic backscattered measurements associated with approximately the same scattering volume and transmission loss. We assume that the sonar source level remains constant during the time of the experiment. There is some temperature dependence in transmission loss but, given the temperature variation of the experiment of order 10 °C, it should be of order no more than 5% (Deines, 1999).

D. Combination Backscattering Meter and Fluorometer (BB2F)

This is a combination sensor, manufactured by WET Labs of Philomath, OR, for concurrent determination of optical backscattering at 470 and 700 nm and chlorophyll-a fluorescence. These are all performed within the same optical scattering volume. This sensor system will be used to examine the potential role of zooplankton and sedimentary particle induced scattering in the received acoustic signal. The system has been used successfully in the Layered Organization of the Coastal Ocean experiment (LOCO) field experiments (Goodman and Wang, 2007; Wang and Goodman, 2010) to identify regions of thin plankton layers and relate these to the local turbulence and fine scale fields.

IV. MerMADE OBSERVATIONS

Measurements were carried during the May 9, 2007 deployment of the Merrimack River Mixing and Divergence Experiment (MerMADE). The site of this experiment is characterized by extremely large salinity induced turbulence due to the discharge of the Merrimack River into the Gulf of Maine. A comprehensive description of the study site and observations of turbulence in the Merrimack River can be found in MacDonald *et al*. (2007). The T-REMUS was deployed close to the river mouth from which it navigated downstream in a 1° yoyo profiling pattern at a velocity 1 m/s. This was done in order to sample both the vertical and horizontal structure of the plume. All quantities, both acoustic and turbulent, are averaged over a vertical distance of 0.2 m, which correspond to an average of approximately 12 m horizontally.

In Fig. 2 shown are contour plots of (a) dissipation rate, ε; (b) diffusion rate of temperature variance, χ_T; (c) chlorophyll-a concentration, Chl-a; (d) optical scattering cross

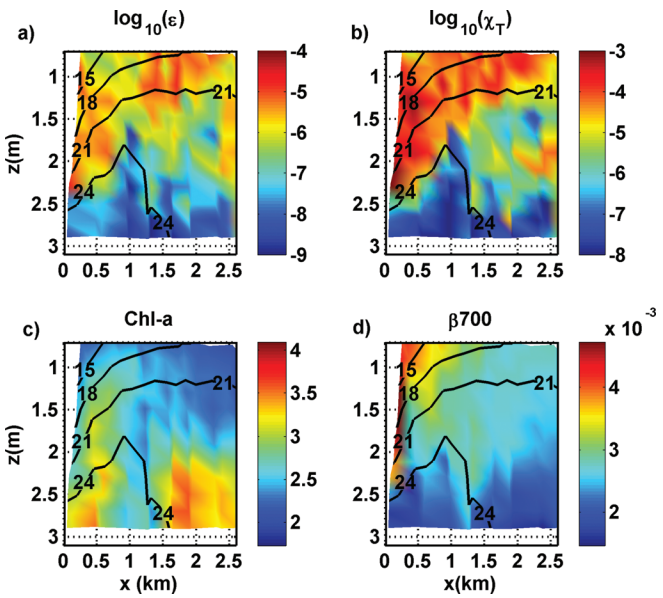

FIG. 2. Contour plots of (a) turbulent kinetic energy dissipation rate, ε, units of Watts per kilogram; (b) diffusion rate of temperature variance, χ_T, units of degrees Centigrade squared per second; (c) chlorophyll-a, Chl-a, units of micrograms per liter; (d) optical scattering cross section per volume at a wavelength of 700 nanometers, β 700, units of inverse meters. These quantities are plotted vs downstream distance, x, in units of kilometers and depth, z, in units of meters. The downstream distance of the track of the T-REMUS, x, is referenced to the initial set of T-REMUS measurements at $x=0$ km and is located at latitude = 42.8175 N, longitude = −70.8034 E. The black lines indicate the value of a density surface, $\sigma_t = \rho - 1000$.The color bars have a logarithmic to the base 10 scaling.

section per volume at a wavelength of 700 nm, β 700. We take the downstream distance of the track of the T-REMUS, x, referenced to the beginning at $x=0$ km of our measurements and located at latitude 42.8175 N, longitude $=-70.8034$ E. The black lines indicate the value of a density surface, $\sigma_t = \rho - 1000$. The data used to construct these contours are taken from 18 T-REMUS yoyo profiles. From Fig. 2(a) and Fig. 2(b), we see that ε and χ_T span 5 orders of magnitude, while, from Fig. 2(c) and Fig. 2(d), Chl-a and β700 span only a factor of 3. As seen in Fig. 2(c) and Fig. 2(d), the Chl-a and β 700 fields indicate that the plume extends to approximately the $\sigma_t = 24$ kg/m^3 isopycnal, with significant Chl-a concentration below this isopycnal and significant β700 values above. This is not unexpected since the Merrimack River tends to carry sediments but not phytoplankton, with the latter typically present in the adjacent Gulf of Maine water. The spatial extent and degree of variation of concentration of Chl-a and β700 will be important clues to the role in which zooplankton and sedimentary particles play in the acoustic scattering process. This will be further elaborated in Sec. VII.

As indicated in Fig. 2, from $x=0$ to $x=1$ km, the plume shallows. This results from the Merrimack River exiting into the heavier and saltier Gulf of Maine water. Beyond $x=1$ km, turbulent mixing results in the plume deepening.

The two turbulent quantities, ε, and χ_T, of Fig. 2(a) and Fig. 2(b), respectively, have been calculated using the standard physical oceanographic and fluid dynamic spectral techniques (Batchelor, 1993; Gregg, 1987; Dillon and Calwell, 1980). We fit velocity gradient and temperature gradient spectral estimates over a wavenumber range of 8 to 20 cpm to Nasmyth (1970) and Kolmogorov-Batchelor spectra (Dillon and Caldwell, 1980), respectively, from which we obtain, ε, and χ_T, respectively. We use 20 spectral samples resulting in 40 degress of freedom for each ε and χ_T estimate. This approach implicitly assumes that the turbulent field is locally isotropic. Yamazaki and Osborn (1990) have developed criteria for when this is expected. The criteria is based on the buoyant Reynolds number, R_{eb}, defined by

$$\mathrm{R}_{eb} = \frac{\varepsilon}{\nu N^2} = \left(\frac{l_B}{l_\nu}\right)^{4/3}, \tag{5}$$

where N is the buoyancy frequency,

$$N = \sqrt{-\frac{g}{\rho_\theta}\frac{\partial \rho_\theta}{\partial z}};$$

the density, ρ_θ, is the potential density, which is the water density referenced to surface pressure (Picard and Emery, 1990). The length scales l_B, l_v are defined, respectively, by

$$l_B = \left(\frac{\varepsilon}{N^3}\right)^{1/2},$$
$$l_v = \left(\frac{\varepsilon}{\nu^3}\right)^{-1/4},$$

and represent the buoyancy and viscous length scales in a stratified turbulent field (Tennekes and Lumley, 1972). According to classical turbulence theory (Batchelor, 1993; and Tennekes and Lumley, 1972), isotropy in the turbulent field is expected when $l_B \gg l_\nu$. Yamazaki and Osborn (1990) confirmed this result by finding that, when $\mathrm{R}_{eb} < 20$, there was a 35% error in the estimation of isotropy. The value of $\mathrm{R}_{eb} = 20$ corresponds to $l_B/l_\nu \approx 10$, the order of magnitude criteria for isotropy in classical turbulence theory. Yamazaki and Osborn (1990) found that fully developed isotropic turbulence was most likely for $\mathrm{R}_{eb} > 100$.

Because of the very large stratification of the Merrimack River plume, particularly in the region $x<1$ km, large values of ε do not necessarily imply isotropic turbulence. In Fig. 3 we show contour plots of the gradient Richardson number, R_i, Fig. 3(a), and the buoyancy Reynolds number, R_{eb}, Fig. 3(b). The gradient Richardson number is defined by

$$\mathrm{R}_i = \frac{N^2}{\left(\frac{\partial \bar{u}}{\partial z}\right)^2 + \left(\frac{\partial \bar{v}}{\partial z}\right)^2}$$

and is a measure of the dynamic stability of the flow field, with $\mathrm{R}_i < 1/4$, indicating shear instability (Miles, 1961; Howard, 1961) and the likelihood of continuous turbulence. The denominator of the above equation is the square of the total mean velocity shear in the vertical direction.

From Fig. 3(a), for $\sigma_t < 24$ kg/m^3, typically $\mathrm{R}_i < 1/4$. At ranges greater than $x>1.5$ km and depths below 1.5 m, R_i begins to increase above the critical value of 1/4. Figure 3(b) indicates $R_{eb} > 100$ over much of plume except for the range at which the plume depth extent is a minimum, $x<0.9$ km and $z>2$ m, where intermittency of the turbulent field is

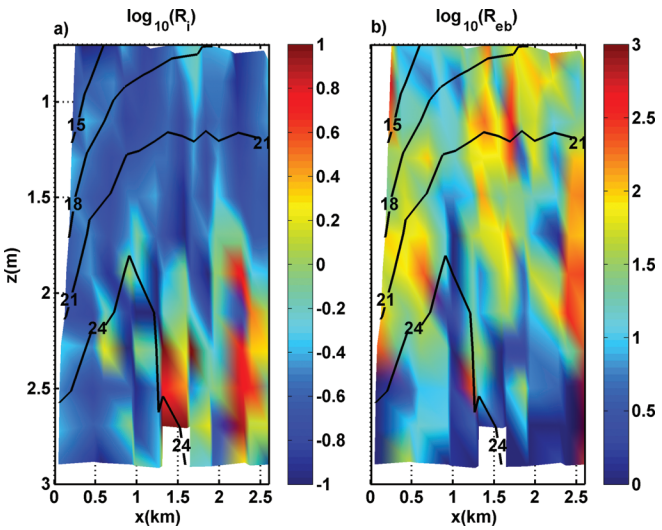

FIG. 3. Contour plots of (a) the gradient Richardson number, R_i, and (b) buoyancy Reynolds number, R_{eb}. These are defined by $\mathrm{R}_i = N^2/(\partial\bar{u}/\partial z)^2 + (\partial\bar{v}/\partial z)^2$ and $R_{eb} = \varepsilon/\nu N^2$; ε is the turbulent kinetic energy dissipation rate; ν, the kinematic viscosity; N, the buoyancy frequency; and $(\partial\bar{u}/\partial z), (\partial\bar{v}/\partial z)$ the along and cross track mean velocity gradients, respectively. These quantities are plotted versus downstream distance, x, in units of kilometers, and depth, z, in units of meters. The downstream distance of the track of the T-REMUS, x, is referenced to the initial set of T-REMUS measurements at $x=0$ km and is located at latitude $=42.8175$ N, longitude $=-70.8034$ E. The black lines indicate the value of a density surface, $\sigma_t = \rho - 1000$.The color bars have a logarithmic to the base 10 scaling.

expected. Thus, we conclude that over most of the plume use of the standard spectral techniques to estimate ε, χ_T should produce minimal errors due to anisotropy.

From Sec. II we see that the key statistical turbulent quantities for input into estimating the temperature and salinity scattering cross section per volume is $\gamma_{T,S} = (\chi_{T,S}/\sqrt{\varepsilon}) \times \exp[-4q(k/k_{T,S})^2]$. Since χ_S cannot be inferred directly from our suite of measurements but, as discussed previously, χ_T can, we will use the approximation $\chi_S = (\partial\bar{S}/\partial T)^2 \chi_T$, which results in the relationship

$$\gamma_S = \left(\frac{\partial \bar{S}}{\partial \bar{T}}\right)^2 \tilde{\gamma}, \tag{6}$$

where

$$\tilde{\gamma} = \frac{\chi_T}{\sqrt{\varepsilon}} \exp[-4q(k/k_S)^2]$$

and $(\partial\bar{S}/\partial\bar{T})$ is the mean local gradient of salinity with respect to temperature. Using Eq. (6) is based on the requirement that, locally, the mean T/S relationship is linear, i.e., $\partial\bar{S}/\partial\bar{T}$ is constant over the depth range in which the turbulent averages contained in $\tilde{\gamma}$ are estimated. MacDonald *et al.* (2007) have used the linearity of the T/S relationship to estimate ε by their control volume method.

To examine the validity of this approximation, we plot in Fig. 4a contour map of $10\log_{10}(\tilde{\gamma})$ in a T, S coordinate system. We see that $\tilde{\gamma}$ varies by over 2 orders of magnitude. The lines, labeled A, B, C, D show the T/S relationship for T-REMUS yoyo profiles obtained from the FASTCAT CTD at downstream distances of $x = 0.16$ km, $x = 1.0$ km, $x = 1.6$ km, $x = 2.4$ km. The white lines indicate the nonlinear region of the T/S relationship. Lines A and B are approximately linear over the entire range of T, S values while lines C and D deviate from linearity only above $\sigma_t = 22$ kg/m^3.

We also see that the linear T/S approximation is valid for values of $10\log_{10}(\tilde{\gamma})$ over two orders of magnitude, namely, in the region where -5 dB$> 10\log_{10}(\tilde{\gamma}) > -25$ dB. Deviation from linearity, as indicated by the white line segments for cases C and D, occurs near the base of the plume, where, typically, values of $10\log_{10}(\tilde{\gamma}) < -25$ dB, and where, from Eqs. (2), (3), and (4), the scattering is expected to be 2 orders of magnitude smaller there than that in the upper region. Thus, we expect $\chi_S = (\partial\bar{S}/\partial T)^2 \chi_T$ to be valid above the bottom transition plume seawater interface.

We now have all of the quantities necessary to estimate the turbulent induced scattering cross section terms in Eq. (1). In Fig. 5(a) we show the sum of the scattering strength, S_{TS}, associated with temperature induced turbulence, term (I) of Eq. (1), and an upper bound for the temperature/salinity cross spectral term (II) of Eq. (1), given by $S_{TS} = 10\log_{10} \times(\sigma_T + 2\sqrt{\sigma_T \sigma_S})$. In Fig. 5(b) we show the salinity turbulence scattering strength, $S_S = 10\log_{10}(\sigma_S)$. Comparing Fig. 5(a) and Fig. 5(b), we see that over the entire range of the experiment S_{TS} is at least 30 dB smaller than S_S. This result occurs because the acoustic frequency of the ADCP, $f = 1.2$ MHz, results in the exponential term of Eq. (4) for γ_T being very small, i.e., $\exp[-4q(k/k_T)^2] \ll 1$. For the case of salinity induced scattering, that term is given by $\exp[-4q(k/k_S)^2] \approx 1$.

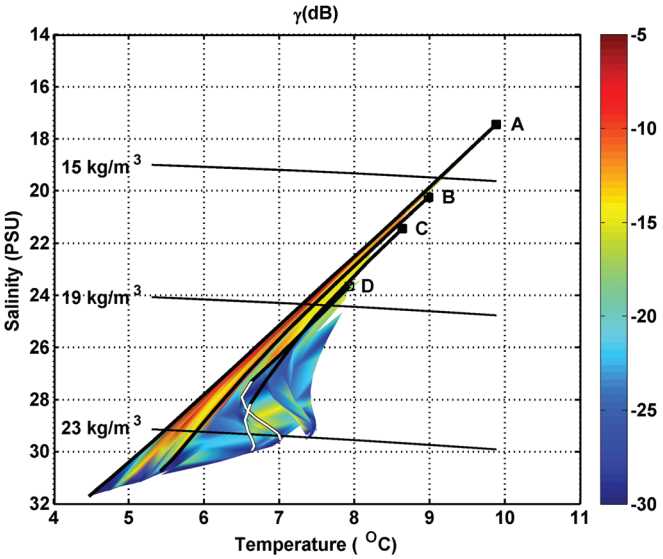

FIG. 4. Contour map of $10\log_{10}(\tilde{\gamma})$ in a T, S coordinate system. The quantity $\tilde{\gamma}$ is defined by $\tilde{\gamma} = \chi_T/\sqrt{\varepsilon}\exp[-4q(k/k_S)^2]$, where χ_T is diffusion rate of temperature variance; ε, the turbulent kinetic energy dissipation rate; k, the acoustic wavenumber and k_S, the Batchelor wavenumber, the latter given by $k_S = (\varepsilon/\nu D_S^2)^{1/4}$, with D_S, the molecular diffusivity of salt; ν is the kinematic viscosity of water; and q, a dimensionless constant, estimated to be ~3.7. The lines, labeled A, B, C, D show the T/S relationship obtained from the FASTCAT CTD at mean downstream distances of $x = 0.16$ km, $x = 1$ km, $x = 1.6$ km, $x = 2.4$ km. The light black lines indicate the value of a density surface, $\sigma_t = \rho - 1000$. The color bar is scaled in dB.

Before proceeding to the details of the statistical correlation technique employed to estimate the contribution of σ_S to the received acoustic signal, we need to examine how coincident the observed acoustic and environmental

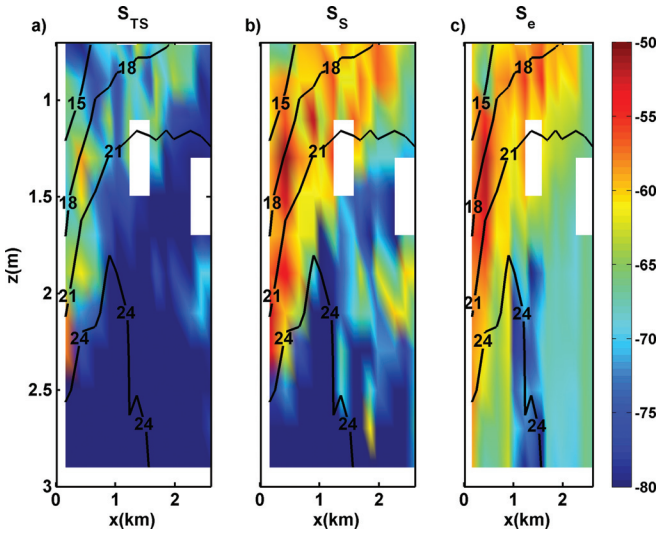

FIG. 5. Contour plots of (a)$S_{TS} = 10\log_{10}(\sigma_T + 2\sqrt{\sigma_T\sigma_S})$, the scattering strength from temperature turbulence and the temperature salinity covariance; (b)$S_S = 10\log_{10}(\sigma_S)$, the scattering strength from salinity turbulence, and (c) $S_e = 10\log_{10}(\sigma_e)$, the estimated scattering strength. These quantities are plotted vs downstream distance, x, in units of kilometers, and depth, z, in units of meters. The downstream distance of the track of the T-REMUS, x, is referenced to the initial set of T-REMUS measurements at $x = 0$ km and is located at latitude = 42.8175 N, longitude = −70.8034 E. The black lines indicate the value of a density surface, $\sigma_t = \rho - 1000$.The white areas are regions where estimations of σ_S,σ_T, and $\sigma_e$have less than 40 deg of freedom. The color bar, located on the rand hand side of the figures, is scaled in dB.

measurements are. For the acoustic observations we use the returns from the first acoustic bin of both the upward and downward looking ADCP sonar systems. This yields a standoff range of 1.1 m for the scattering volume located 20° from the vertical. Since the angle of the yoyo track AUV track is 1° and the vehicle moves at 1 m/s relative to the water, the distance between the location of the source of the acoustic scattering and the turbulence measurements is approximately 60 m horizontally. The issue, then, is whether the σ_S estimate, given by Eqs. (2), (3), and (4), is correlated over that distance and can be effectively considered as coincident with the turbulence measurements.

The correlation coefficient of $\gamma_s(x,z)$, obtained from adjacent AUV yoyo profiles at the same depth, z, is defined by

$$r = \frac{\langle \gamma_s'(x_1,z)\gamma_s'(x_2,z)\rangle}{\langle\{\gamma_s'(x_1,z)\}^2\rangle^{1/2}\langle\{\gamma_s'(x_2,z)\}^2\rangle^{1/2}}.$$

The prime indicates a fluctuating quantity, defined by $(X)' = (X) - \langle(X)\rangle$, with the angle brackets the mean value of the quantity. Each pair, $\gamma_s'(x_1,z),\gamma_s'(x_2,z)$, is located at the same depth, but separated horizontally at distances x_1, x_2, respectively. In Fig. 6(a) the correlation coefficient, r, versus depth, z, is presented and, in Fig. 6(b), the corresponding horizontal separation distance, $d = x_2 - x_1$, in terms of its depth dependence, $d(z)$. The light gray line in Fig. 6(a) is the correlation coefficient at the 90% confidence limit for random, log normal noise. A log normal distribution is used for the noise based on the fact that ε and χ tend to be log normal, and on the observed probability density function (PDF) presented later in the manuscript and discussed in Sec. VI. Because of the AUV yoyo pattern and pair sampling employed, the separation distance, d(z), increases with depth, z. We can identify a minimum horizontal correlation length and its depth according to where r is significant. From Fig. 6(a), this occurs between $z = 1.1$ m and $z = 2.4$ m. Over that depth interval the minimum horizontal correlation length is given by the value of d, which typically exceeds the 60 m horizontal distance between the acoustic scattering volume and the *in situ* environmental sampling region. This result indicates that the acoustic and turbulence measurements made in the 1.1 to 2.4 m depth range are statistically near coincidental.

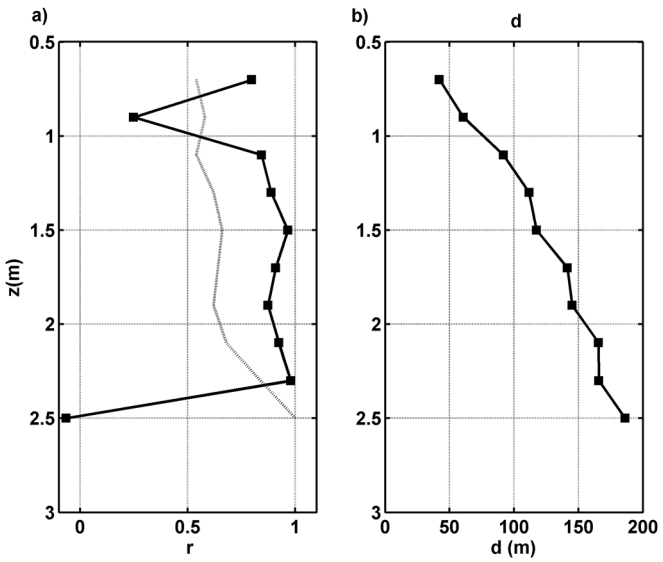

FIG. 6. The spatial structure of the correlation function, $r = \langle \gamma_s'(x_1,z) \times \gamma_s'(x_2,z)\rangle / \langle\{\gamma_s'(x_1,z)\}^2\rangle^{1/2}\langle\{\gamma_s'(x_2,z)\}^2\rangle^{1/2}$. The prime indicates a fluctuating quantity defined by $(X)' = (X) - \langle(X)\rangle$, with the angle brackets the mean value of the quantity. Each pair, $\gamma_s'(x_1,z),\gamma_s'(x_2,z)$, is located at the same depth, but separated horizontally at distances x_1, x_2, respectively. The quantity γ_s is given by $\gamma_s = (\chi_s/\sqrt{\varepsilon})\exp[-4q(k/k_S)^2]$, where χ_s is diffusion rate of salinity variance; ε, the turbulent kinetic energy dissipation rate; k, the acoustic and k_S, the Batchelor wavenumber, the latter given by $k_S = (\varepsilon/\nu D_S^2)^{1/4}$, with D_S, the molecular diffusivity of salt; ν is the kinematic viscosity of water; and q, a dimensionless constant, estimated to be ~3.7. In (a) the correlation coefficient, r, vs depth, z, is presented and in (b), the corresponding horizontal separation distance, $d = x_2 - x_1$, depth dependence, $d(z)$. The light gray line in (a) is the correlation coefficient at the 90% confidence limit for random, log normal noise.

V. STATISTICAL APPROACH

By using the first bin of the T-REMUS ADCP sonar system, the uncalibrated intensity observations, I, are characterized by approximately the same transmission loss, the same scattering volume size, and the same incident power. Thus, for this case, we can relate the scattering cross section per unit volume, σ, to the received intensity, I, in the linear form $\sigma = \alpha I$, where α is the calibration coefficient. If the received intensity is the result of volume scattering from salinity turbulence then

$$\sigma = \alpha I = \sigma_S. \tag{7}$$

Thus, measurements of I and σ_S can be used to estimate the calibration coefficient, α. If the scattering from the Merrimack River plume is dominated by salinity turbulence, the calibration coefficient, α, should be constant as a function of location, even though the received acoustic intensity varies.

The mean and fluctuating components of Eq. (7) can be written

$$\bar{\sigma} = \alpha\bar{I} = \bar{\sigma}_S, \tag{8a}$$

$$\sigma' = \alpha I' = \sigma_S', \tag{8b}$$

where the overbar is used interchangeable with the angle brackets to indicate a mean value. Using measurements of σ_S and I, we can estimate the calibration coefficient, α, by minimizing the magnitude of error function, $E = \sigma_e - \sigma_S$, with respect to α, with $\sigma_e = \alpha I$, the estimated scattering cross section per unit volume from salinity turbulence. This results in

$$\alpha = \frac{\langle(\sigma_S')I'\rangle}{\langle(I')^2\rangle}. \tag{9}$$

The accuracy of this measurement can be assessed using the mean error,

$$E_m = \frac{\bar{E}}{\bar{\sigma}_S} = \frac{|\bar{\sigma}_S - \bar{\sigma}_e|}{\bar{\sigma}_S}, \tag{10a}$$

and variance error,

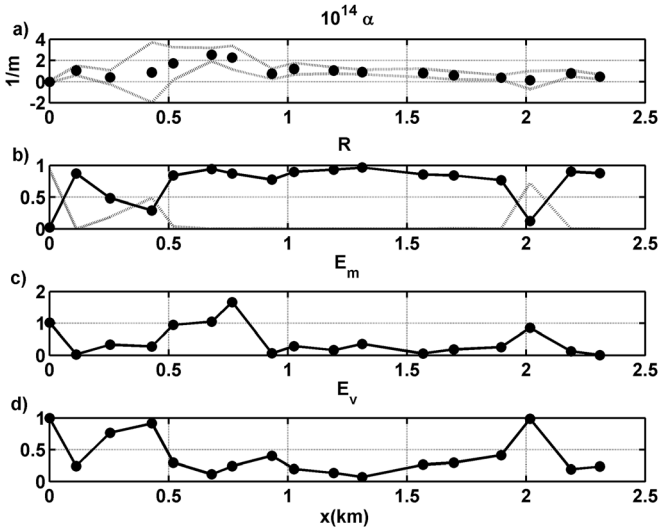

FIG. 7. Downstream range plots of (a) α; (b) R; (c) E_m; (d) E_V. These are given, respectively, by $\alpha = \langle(\sigma_S' I'\rangle / \langle(I')^2\rangle$ $R = \langle\sigma_S' I'\rangle / \langle(\sigma_S')^2\rangle^{1/2}\langle(I')^2\rangle^{1/2}$, $E_m = |1 - R\{\langle(\sigma_S')^2\rangle^{1/2}/\bar{\sigma}_S\}/\{\langle(I')^2\rangle^{1/2}/\bar{I}\}|$, $E_V = 1 - R^2$, with σ_S, the salinity turbulence scattering cross section per volume and I, the received uncalibrated intensity. In (a), the light gray lines are the 95% confidence limits; in(b), the light gray line is the probability of getting a correlation as large as the observed value from random, log normal Gaussian noise.

$$E_V = \frac{|\langle(\sigma_e' - \sigma_S')^2\rangle|}{\langle(\sigma_S')^2\rangle}. \tag{10b}$$

Using Eq. (9), it is straightforward to show that E_m and E_V can be expressed in terms of measurable quantities, namely,

$$E_m = \frac{|\langle\sigma_e - \sigma_S\rangle|}{\bar{\sigma}_S} = \left|1 - R\frac{\left\{\frac{\langle(\sigma_S')^2\rangle^{1/2}}{\bar{\sigma}_S}\right\}}{\left\{\frac{\langle(I')^2\rangle^{1/2}}{\bar{I}}\right\}}\right|, \tag{11a}$$

$$E_V = \frac{|\langle(\sigma_e' - \sigma_S')^2\rangle|}{\langle(\sigma_S')^2\rangle} = 1 - R^2, \tag{11b}$$

where R is the correlation coefficient between the fluctuating salinity cross section per volume, σ_S', and the received uncalibrated intensity, I',

$$R = \frac{\langle\sigma_S' I'\rangle}{\langle(\sigma_S')^2\rangle^{1/2}\langle(I')^2\rangle^{1/2}}. \tag{11c}$$

Equations (11a) and (11b), along with the requirement that the calibration coefficient, α, remain constant, will be used to find locations where salinity turbulence dominates the scattering.

VI. RESULTS

We now apply the approach of Sec. V to the MerMADE data set. In Figs. 7(a)–7(d) we show, respectively, estimates of the calibration coefficient, α, the correlation coefficient, R, the mean error, E_m, and the variance error, E_V, for each of the first 17 yoyo profiles of the MerMADE data. In Fig. 7(a) the light gray lines are the 95% confidence limits; in Fig. 7(b) the light gray line is the probability of getting a correlation as large as the observed value from random, log normal, Gaussian noise. In the interval from $x = 0.9$ km to $x = 1.8$ km, the calibration coefficient, α, has a mean value of $\bar{\alpha} = 8.0 \times 10^{-15}$ m^{-1} with a standard deviation of $\langle(\alpha')^2\rangle^{1/2} = 3.0 \times 10^{-15}$ m^{-1}, a correlation coefficient of $R = 0.9$, a mean error of $\bar{E}_m = 0.09$, and a variance error of $E_V = 0.12$. Figure 8 shows three example profiles of σ_S (black circles) and σ_e (black line) in that range interval. These are located, respectively, at (a) $x = 1$ km; (b) $x = 1.2$ km; (c) $x = 1.3$ km. Figure 9 contains a plot of σ_S (black

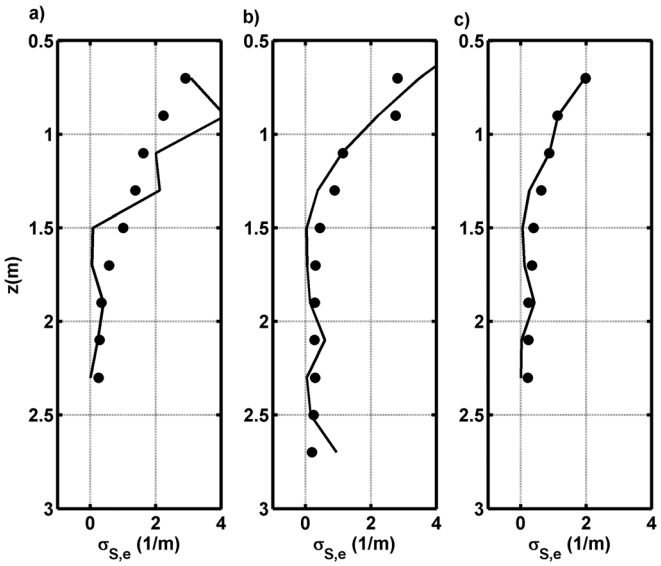

FIG. 8. Three example profiles of σ_S, σ_e. The salinity turbulence scattering cross section per volume, σ_S, is indicated by the black circles. The estimated scattering cross section per volume, σ_e, is indicated by the black line. These profiles are located, respectively, at (a) $x = 1$ km; (b) $x = 1.2$ km; (c) $x = 1.3$ km.

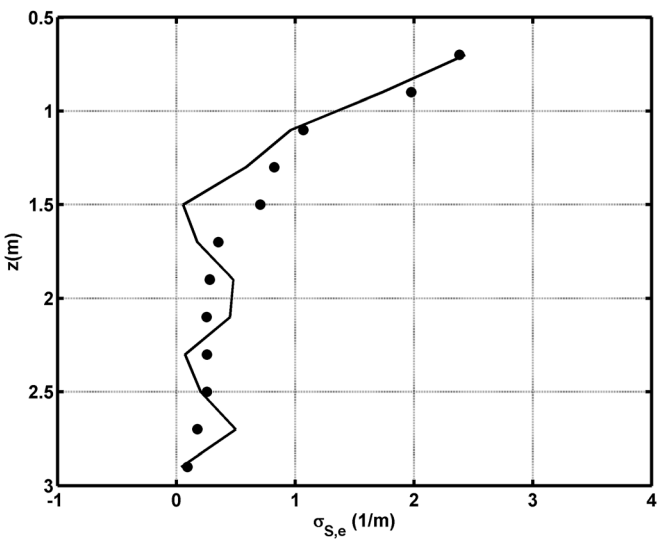

FIG. 9. Average profiles of σ_S and σ_e between $x = 0.9$ km to $x = 1.8$ km. The salinity turbulence scattering cross section per volume, σ_S, is indicated by the black circles. The estimated scattering cross section per volume, σ_e, is indicated by the black line. In this interval the calibration coefficient, α, has a mean value of $\bar{\alpha} = 8.0 \times 10^{-15}$ m^{-1} with a standard deviation of $\langle(\alpha')^2\rangle^{1/2} = 3.0 \times 10^{-15}$ m^{-1}, a mean error, $\bar{E}_m = 0.09$, and variance error, $E_V = 0.12$.

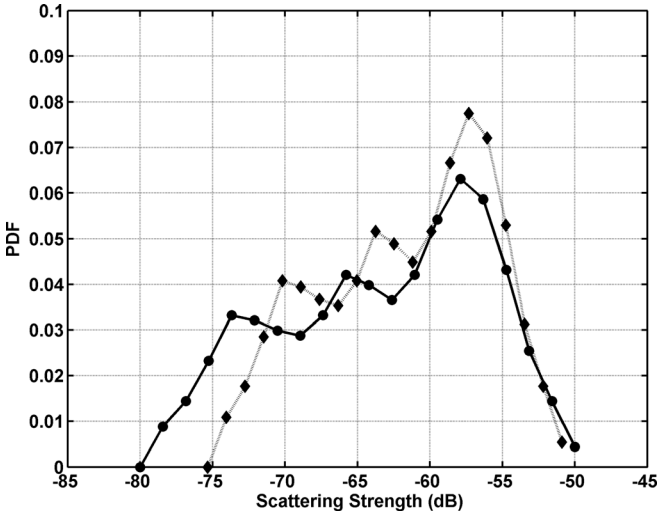

FIG. 10. The observed probability density function (PDF). Shown are the PDF for salinity turbulence scattering cross section per volume, σ_S, black circles, in units of dB; and the estimated scattering cross section per volume, σ_e, black diamonds, in units of dB.

circles) and σ_e (black line), averaged between $x=0.9$ km and $x=1.8$ km.

From Figs. 7(c) and 7(d), outside of the interval $x=0.9$ km to $x=1.8$ km, we see instances of E_m and E_V approaching 1, although there are some locations where they are much less than 1 and $\bar{\alpha} \approx 8 \times 10^{-15}$ m^{-1}. Over all about 50% of all of the observed data indicate values of $\alpha \approx 8 \times 10^{-15}$ m^{-1} and $E_m, E_V < 0.25$.

In Fig. 5(c) we have plotted a contour map of the estimated salinity turbulence scattering strength $S_e = 10\log_{10}(\sigma_e)$. Comparing Fig. 5(b) and 5(c) we see strong qualitative agreement between S_e and S_S, particularly for $\sigma_t < 24$ kg/m^3. For $\sigma_t > 24$ kg/m^3, there is less agreement, which from Fig. 3(b) and Fig. 4, is not unexpected since the assumptions of isotropy for the turbulent field and linearity for the T/S relationship begin to break down there.

Given these results and the statistical nature of this approach, we plot in Fig. 10 the measured normalized histogram, i.e., the estimated PDF, for σ_S and σ_e for all of the data collected. The PDF for both σ_S (black circles) and σ_e (black diamonds) show a skewed, log normal distribution, with both quantities having larger tails at their lower values. They both peak at very close values (−58 dB) and have very similar mean and variances, namely,

$$\bar{S}_S = -63.2\,\text{dB}, \quad \langle (S_S')^2 \rangle^{1/2} = 7.2\,\text{dB},$$
$$\bar{S}_e = -62.0\,\text{dB}, \quad \langle (S_e')^2 \rangle^{1/2} = 5.9\,\text{dB}.$$

VII. OTHER SOURCES OF SCATTERING

Our results have indicated that over 50% of the experimental area and, in particular, over downstream distances of $x=0.9$ km to $x=1.8$ km, salinity turbulence is primarily responsible for the acoustic scattering observed. However, within a fast moving freshwater buoyant plume such as the Merrimack River, other possible sources of acoustic scattering can exist. These sources include (1) bubbles; (2) zooplankton; and (3) sedimentary particles.

For scattering contributions due to bubbles, this should be insignificant. The mean wind speed during the experiment was very light, less than three knots, and resulted in a very calm, flat sea surface, with no visual breaking waves or white caps. Also, in the experimental site there were no observed surface convergences or surface "boils" which might be able to entrain air bubbles.

We can use output from the Chl-a and β 700 channels of the BB2F sensor system to examine the potential of zooplankton and particulates, respectively, as sources of scattering. In late spring, when the MerMADE experiment took place, the Chl-a concentration in the Gulf of Maine area where the Merrimack river exits has been known to correspond very well with the biomass of Calanus finmarchicus (Durbin *et al.*, 1995; Ashjian *et al.*, 2001), a very common copepod in the region. Expecting correspondence of the availability of phytoplankton as its food source and using Chl-a concentration output from the BB2F sensor system, as indicated in Fig. 2(c), significant Chl-a concentration only occurs below the buoyant plume, i.e., $\sigma_t > 24$ kg/m^3.

Bunt *et al.* (1999) have shown that optical backscattering data at non-saturating levels are a good indicator of particulate density. There has been extensive research on the use of optical scattering data to infer sediment transport concentration (for example, Chanson *et al.*, 2007). Of the two wavelengths of the BB2F sensor system, namely, 470 and 700 nm, the 700 nm channel is much less sensitive to dissolved organic material and phytoplankton (Bukata *et al.*, 1995). From Fig. 2(d) the β700 signal decreases significantly with downstream distance, particularly in the range where salinity scattering dominates, namely, $x=0.9$ km to $x=1.8$ km.

But a more quantitative basis for ruling out the importance of scattering from these sources is the nature of statistical variation of the received intensity signal. In Fig. 10 the PDF of the scattering strength from salinity turbulence, $S_S = 10\log_{10}(\sigma_S)$, and that of the estimated scattering strength, S_e, show a variation of three orders of magnitude (30 dB), with close values for their mean and standard deviation. On the other hand, Chl-a and β 700, the linear surrogates for zooplankton and sedimentary particulates, respectively, from Fig. 2(c) and Fig. 2(d), have variations of only a factor of 3.

VIII. SUMMARY AND CONCLUSIONS

The region where the Merrimack River exits into the Gulf of Maine is characterized by a strong fresh water, saline water interface. It is a near ideal site to examine whether salinity fluctuations can produce observable acoustic scattering. During the Merrimack River Mixing and Divergence Experiment (MerMADE), the T-REMUS vehicle collected a unique set of near coincident acoustic and environmental data. Instruments on board the T-REMUS included two upward and downward looking 1.2 MHz ADCP sonar systems, a FASTCAT CTD, and the RMMS turbulence package. The vehicle was employed in a yoyo mode allowing a

detailed spatial characterization of the acoustic and environmental fields. A statistical correlation approach was employed to examine the relationship between a modeled salinity induced scattering cross section per volume based on classical turbulence theory, σ_s, and the received uncalibrated acoustic intensity, I. The technique involves estimation of the calibration coefficient, α, by minimizing the error function, $E = |\langle \sigma_s - \sigma_e \rangle|$, with $\sigma_e = \alpha I$, the estimated scattering cross section per unit volume. The calibration coefficient, α, should be approximately constant over those regions where salinity turbulence dominates as the source of acoustic scattering. In addition, for that case, the values of error functions $E_m = E/\sigma_S$ and $E_V = \left|\langle (\sigma'_e - \sigma'_S)^2 \rangle / \langle (\sigma'_S)^2 \rangle\right|$ should be much less than 1. It is observed that over a segment of the data from downstream distance $x = 0.9$ km to $x = 1.8$ km that $\alpha \approx 8.0 \times 10^{-15}$ m^{-1} $\pm$ 3×10^{-15} m^{-1} and $E_m = 0.09$, $E_V = 0.12$ The PDF for σ_e and σ_S are qualitatively similar with very close values of their mean and standard deviation.

We have presented evidence that over most of plume other sources of scattering such as that from bubbles, zooplankton, and sedimentary particles are not expected to play a significant role in the scattering, although there are specific regions where zooplankton or sedimentary particles could be important.

The largest deviation of the calibration constant, α, occurs in the range $x = 0.5$ km to $x = 0.8$ km and is characterized by $E_m \gtrsim 1$. There, the correlation coefficient is significant with $R \gtrsim 0.8$, which results in $E_V \lesssim 0.25$. However, the result that $E_m > 1$, from Eq. (11a), implies that $\{\langle (\sigma'_S)^2 \rangle^{1/2} / \bar{\sigma}_S\} / \{\langle (\hat{I}')^2 \rangle^{1/2} / \bar{I}\} \gtrsim 1$. Thus, there is a wider range of variation of the modeled turbulent salinity scattering cross section per volume, σ_S, relative to its mean than that of the acoustic intensity, I, relative to its mean. This suggests that in the range $x = 0.5$ km to $x = 0.8$ km the scattering may be the result of salinity turbulence, but not modeled by classical isotropic turbulence theory.

ACKNOWLEDGMENTS

This work was supported by the Office of Naval Research (ONR) through Grants from ONR 322 OA and ONR 322PO and by the Raytheon Company Advanced Study Program Fellowship.

Ashjian, Carin J., Davis, C. S., Gallager, S. M., and Alatalo, P. (**2001**). "Distribution of plankton, particles, and hydrographic features across Georges Bank described using the Video Plankton Recorder," Deep-Sea Res., Part II **48**, 245–282.

Batchelor, G. K. (**1993**). *Homogeneous Turbulence* (Cambridge University Press, New York), Chap. 6, pp 103–132.

Bukata, R. P., Jerome, J. H., Kondratyev, K. Y., and Pozdnyakov, D. V. (**1995**). *Optical Properties and Remote Sensing of Inland and Coastal Waters* (Chemical Rubber Company Press, New York), pp. 147–149.

Bunt, J. A. C., Larcombe, P., and Jago, C. F. (**1999**). "Quantifying the response of optical backscattering devices and transmissometers to variations in suspended particulate matter," Cont. Shelf Res. **19**(9), 1199–1220.

Chanson, H., Takeuchi, M., and Trevethan, M. (**2007**). "Using turbidity and acoustic backscattering intensity as surrogate measures of suspended sediment concentration in a small subtropical estuary," J. Environ. Manage. **73**, 341–350.

Deines, K. L. (**1999**). "Backscatter estimation using broadband acoustic Doppler current profilers," Proceedings of the Institute of Electrical and Electronics Engineers (IEEE) Sixth Working Conference on Current Measurement, San Diego, CA, pp. 249–253.

Dillon, T. M., and Caldwell, D. R. (**1980**). "The Batchelor spectrum and dissipation in the upper ocean," J. Geophys. Res. **85**, 1910–1916.

Durbin, E. G., Campbell, R. G., Gilman, S. L., and Durbin, A. G. (**1995**). "Diel feeding behavior and ingestion rate in the copepod Calanus finmarchicus in the southern Gulf of Maine during late spring," Cont. Shelf Res. **15**, 539–570.

Goodman, L., and Kemp, K. A. (**1981**). "Scattering from volume variability," J. Geophys. Res. **86**, 4083–4088.

Goodman, L. (**1990**). "Acoustic scattering from ocean microstructure," J. Geophys. Res. **95**, 557–573.

Goodman, L., Levine, E. R., and Lueck, R. G. (**2006**). "On measuring the terms of the turbulent kinetic energy budget from an AUV," J. Atoms. Ocean. Tech. **23**, 977–990.

Goodman, L., and Wang. Z. (**2007**). "Turbulence observations in the northern bight of Monterey Bay from a small AUV," J. Mar. Syst. **77**, 441–458.

Gregg, M. (**1987**). "Entropy generation in the ocean by small-scale mixing," J. Phys. Oceanogr. **14**, 688–711.

Howard, L. N. (**1961**). "Note on a paper of John W. Miles," J. Fluid Mech. **13**, 158–160.

Lavery, A. C., Schmitt, R. W., and Stanton, T. K. (**2003**). "High-frequency acoustic scattering from turbulent oceanic microstructure: the importance of density fluctuations," J. Acoust. Soc. Am. **114**, 2685–2697.

MacDonald, D., Goodman, L., and Hetland, R. D. (**2007**). "Turbulent dissipation in a near-field river plume: A comparison of control volume and microstructure observations with a numerical model," J. Geophys. Res. **112**, 1–13.

Miles, J. W. (**1961**). "On the stability of heterogeneous shear flows," J. Fluid Mech. **10**, 496–508.

Nasmyth, P. V. (**1970**). "Ocean turbulence," Ph.D. Thesis, University of British Columbia, Vancouver, BC, pp 1–69.

Oakey, N. S. (**1982**). "Determination of the rate of dissipation of turbulent energy from simultaneous temperature and velocity shear microstructure measurements," J. Phys. Oceanogr. **12**, 256−271.

Oeschger, J., and Goodman, L. (**2003**). "Acoustic scattering from a thermally driven buoyant plume revisited," J. Acoust. Soc. Am. **100**, 1451–1462.

Picard, G. L., and Emery, W. J. (**1990**). *Descriptive Physical Oceanography* (Pergamon, New York), pp. 54−56.

Ross, T., and Lueck, R. (**2003**). "Sound scattering from oceanic turbulence," J. Geophys. Res. Lett. **30**, 1343–1346.

Ross, T., Garrett, C., and Lueck, R. (**2004**). "On the turbulent co-spectrum of two scalars and its effect on acoustic scattering from oceanic turbulence," J. Fluid Mech. **514**, 107–119.

Ross, T., Gaboury, I., and Lueck, R. (**2007**). "Simultaneous acoustic observations of turbulence and zooplankton in the ocean," Deep-Sea Res. I **54**, 143–153.

Seim, H. E., Gregg, M. C., and Miyamoto, R. T. (**1995**). "Acoustic backscattering from turbulent microstructure," J. Atmos. Ocean. Technol. **12**, 367–380.

Tennekes, H., and Lumley, J. L. (**1972**). *A First Course in Turbulence* (MIT Press, Cambridge MA), Chap. 3, pp. 59–103.

Wang, Z., and Goodman, L. (**2010**). "The evolution of a thin phytoplankton layer in strong turbulence," Cont. Shelf Res. **30**, 104–108.

Yamazaki, H., and Osborn, T. (**1990**). "Dissipation estimates for stratified turbulence," J. Geophys. Res. **95**, 9739–9744.